CHAPTER 1

INTRODUCTION

"Astronomy compels the soul to look upwards and leads us from this world to another."

– Plato

1.1 History of our Universe in a nutshell

Humanity has made significant progress from the geocentric belief that the Earth was the centre of the Universe to the realization of our minuscule place in it. In the early 1900s, Lemaitre[34, 35] posited that our Universe originated in a *'Big Bang'* from an infinitely hot and dense state of matter and energy about 13.8 billion years ago. This is now a widely accepted theory about the origin of our Universe. The *Big Bang* was followed by a phase of rapid expansion and cooling that led to the emergence of the elementary particles - electrons, protons and neutrons. These particles eventually combined to form the first neutral atoms - Hydrogen, Helium and trace amounts of Lithium and this phase is known as the *'Recombination Era'*. Almost 370,000 years after the *Big Bang* the Universe entered a phase known as the *'Dark Ages'* when the cosmos became neutral and devoid of luminous sources. Subsequently, after 150-250 million years[36–38], the first stars, referred to as Population III stars, and galaxies began to form, marking the onset of the *'Epoch of Reionization'*. These objects have eluded detection so far, but the hunt continues with newer facilities like the *JWST*[39–45]. Upon the completion of reionization phase, the Universe became visible once more, unveiling the multitude of galaxies, galaxy clusters, and large-scale structures that we see in the night sky. A schematic of the timeline is shown in Figure 1.1.

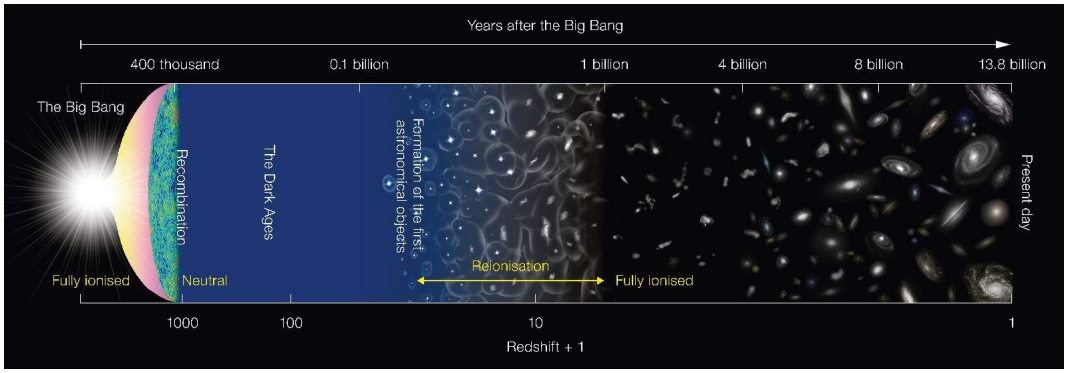

Figure 1.1: **Timeline of our Universe.** A schematic of the beginning and evolution of our Universe from *Big Bang* to present day. Credit: NAOJ

1.2 Brief introduction to galaxies

Galaxies are composites of numerous stars, gas and dust bound together by gravitational forces and typically spanning hundreds of light years across. They also contain an invisible component, known as Dark Matter (hereafter DM), whose presence is only discernible through its gravitational effects on visible matter. Prior to 1920s, our Milky Way (hereafter MW) was perceived as the entire 'observable universe'. But this perception was revolutionized by Edwin Hubble's groundbreaking observations. He discovered a number of galaxies, then termed as nebulae, situated at distances beyond the extent of the MW[46]. He subsequently referred to them as 'island universes' or galaxies. This discovery established him as the pioneer of extragalactic astronomy. Furthermore, Hubble's observations demonstrated that galaxies farther from us exhibit greater recession velocities, providing compelling evidence for the expanding Universe within the framework of *Big Bang* cosmology. Following the discovery in 1924 that Andromeda is distinct galaxy altogether, Hubble introduced a morphological classification of galaxies based on his sample of 400 galaxies[46]. This classification scheme laid the foundation for categorizing modern-day galaxies and is popularly known as the Hubble tuning-fork diagram. As shown in Figure 1.2, galaxies are broadly classified into the following categories:

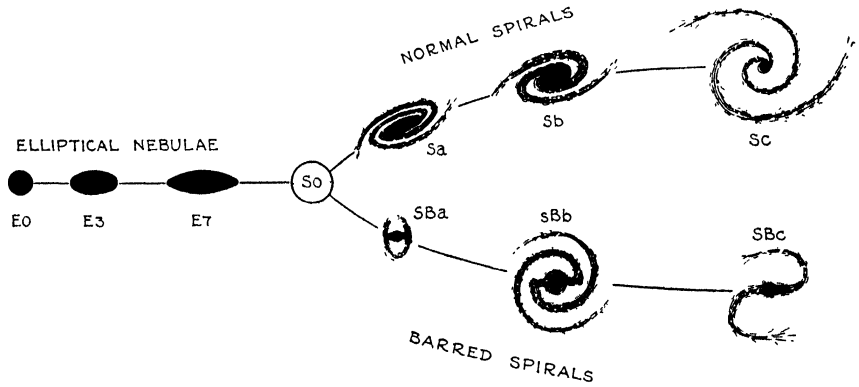

Figure 1.2: **Galaxy morphology.** The classic Hubble's tuning fork diagram showing his classification of regular *'nebulae'*. Credit: The Realm of the Nebulae[47]

- **Elliptical Galaxies**: These are smooth and featureless galaxies, structurally defined and subdivided with increasing ellipticity and denoted as **E*n***, where n ranges from 0 to 7. They usually contain little cold gas and dust with very low levels of star formation. They are populated with old stars as a result of which they emit redder optical colours.

- **Spiral Galaxies**: These are flat and *disky* galaxies usually rich with features like spiral arms, a bar and a bulge. These are subdivided into two classes denoted as **S** and **SB** where the latter indicates the presence of a bar component. Each of the two sub-types is further divided into three classes as **a**, **b** and **c** with a decreasing degree of how tightly the spiral arms are wound around the galaxy. Almost all spiral galaxies are forming stars and contain large reservoirs of cold gas and dust. Due to ongoing star formation and hence the presence of hot and massive stars in these galaxies, they exhibit blue optical colours.

- **Lenticular Galaxies:** These galaxies are apparently an 'intermediate' between ellipticals and spirals. They have a dominating spheroidal component and a weak disk feature and are named **S0**. They may also contain a bar-like feature which are named **SB0**. These galaxies are mostly populated with old stars with very little star formation and hence appear red.

- **Irregular Galaxies**: These galaxies lack any distinctive or regular features. Similar to spirals, these galaxies also contain gas and harbour ongoing star formation.

In addition, elliptical galaxies are usually termed as Early type and spiral galaxies, irregulars as Late type. This is because the Hubble sequence in a sense conveyed an evolutionary sequence from left to right, but there isn't a physical basis for such an evolution. Apart from the above classification, there are a number of galaxies that appear peculiar and quite different due to different ongoing processes such as ongoing merging, harassment due to a fast encounter with another galaxy, ram pressure stripping due to hot intracluster medium, etc. Examples include tadpole galaxies, antennae galaxies, cartwheel galaxies and jellyfish galaxies to name a few (Figure 1.3).

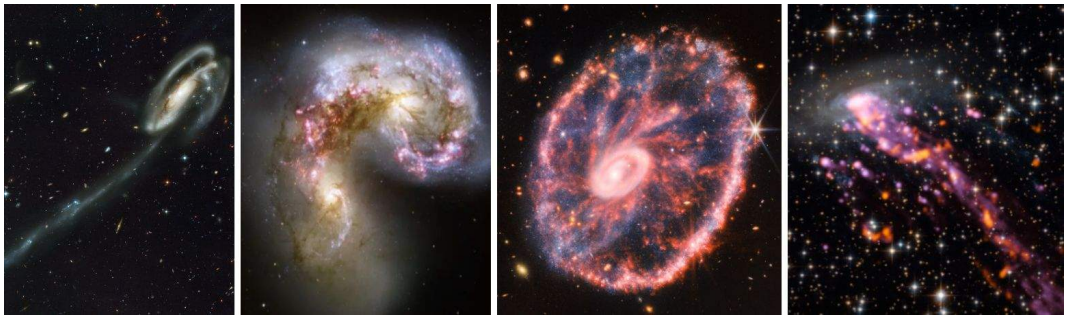

Figure 1.3: **Galaxies with peculiar shapes and structures.** Left to right: Tadpole galaxy Arp 188, Credit: NASA; Antennae galaxies Arp 244, Credit: NASA, ESA, and the Hubble Heritage Team (STScI/AURA)-ESA/Hubble Collaboration; Cartwheel galaxy PGC 2248, Credit: NASA, ESA, CSA, STScI, Webb ERO Production Team; Jellyfish galaxy ESO 137-001, Credit: ALMA (ESO/NAOJ/NRAO), Jachym et al. [48]

1.3 Galaxy formation: A general understanding

Research conducted over the past century has revealed a wealth of information and deepened our understanding of the workings of our Universe. Numerical simulations such as Millennium[49], Illustris[50–53], EAGLE[54], GADGET[55, 56] and others have been largely successful in modelling the observable Universe (Figure 1.4). The Universe started out largely with a uniform density embedded with small-scale fluctuations which later on grew due to gravitational attraction. The signatures of these fluctuations can be found imprinted in the Cosmic Microwave Background Radiation (CMBR) - the residual thermal radiation following the *Big Bang*. The growth and evolution of fluctuations led to the emergence of an interconnected network of filamentary structures, nodes and voids, known as the *Cosmic Web* (Figure

1.4), which serves as the *'backbone'* of our Universe. This is where galaxies or clusters/superclusters of galaxies form and evolve.

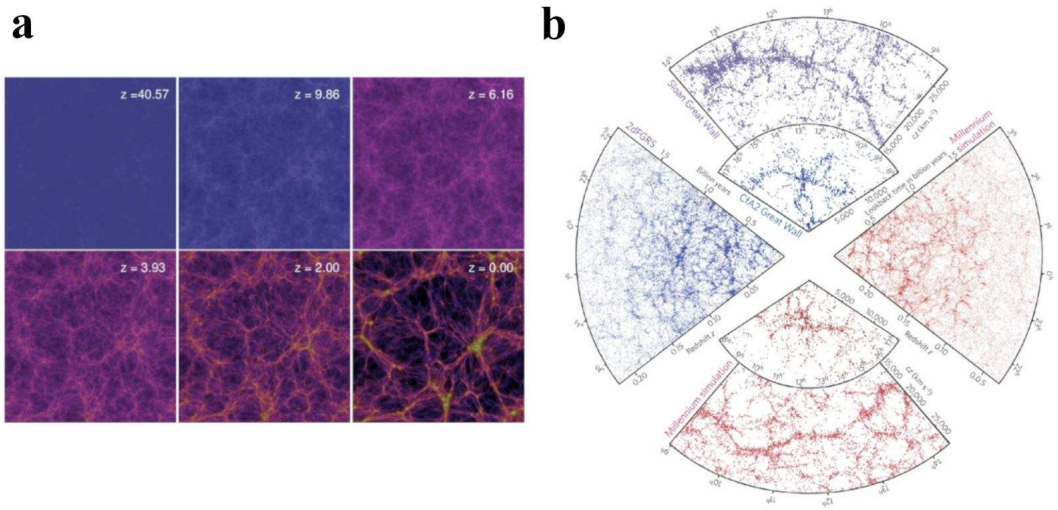

Figure 1.4: **Structure formation from simulations and comparison with observations. a**: This is a simulation[57] using GADGET 3 code[58] from z∼40 to present day which depicts structure formation from a seemingly large scale uniform distribution of matter in the Universe. **b**: This shows a comparison[59] of distribution of galaxies from Sloan Digital Sky Survey (SDSS) and those generated by the Millennium simulation[49].

In the widely accepted Lambda Cold Dark Matter (ΛCDM) paradigm of our Universe, galaxies grow hierarchically, i.e. smaller galaxies combine to form bigger ones which is also accompanied by cold gas accretion from the *Cosmic Web* [9, 60]. Within this cosmological framework, it is believed that the DM halos collapse and come into place first which is then followed by the infall of baryons into these DM halos[61, 62]. Stars and galaxies started to form later on when the neutral gas clouds condensed and collapsed further leading to the fusion of Hydrogen in their cores. Below, we lay down a very brief outline of how the broad classes of Elliptical and Disk galaxies form (Figure 1.5).

- **Formation of Elliptical/Spheroidal galaxies:** Two pathways are often used to explain the formation of this class of galaxies. The first is the *monolithic collapse* scenario, wherein all the stars in a collapsing gas cloud form within a short time which is comparable to the free-fall timescale of the cloud [63, 64]. This is one of the simplest models to explain the formation of elliptical galaxies but cannot produce realistic ellipticals (more in *Galaxy Formation and Evolution*[65]). Secondly, a

merger driven scenario has been proposed, first by Toomre[66], wherein elliptical galaxies form as a result of merging disk galaxies. This scenario, in line with the ΛCDM hierarchical assembly, is able to produce observationally agreeable ellipticals to a considerable extent[24, 67, 68].

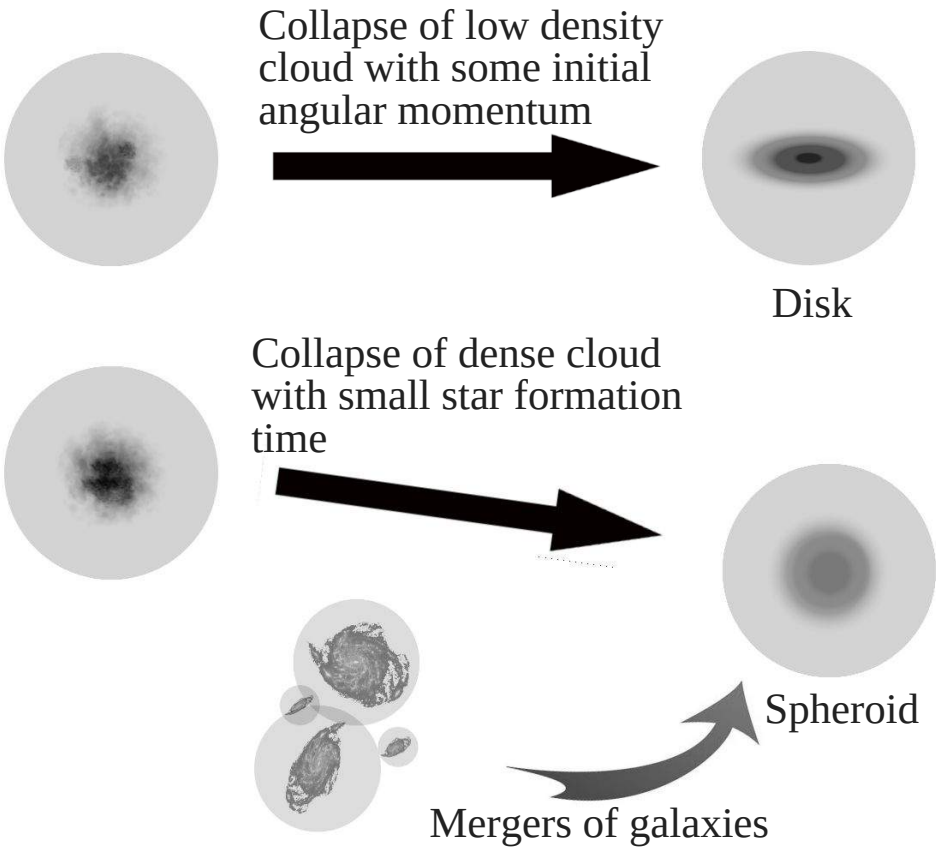

Figure 1.5: **Formation of elliptical/spheroidal and disk galaxies.** As explained above, the schematic depicts the formation of of disk and elliptical galaxies as a result of collapse of gas within DM halos or mergers of galaxies.

- **Formation of Disk galaxies:** Disk galaxies are flat and rotationally supported systems that form as a result of the dissipational collapse of baryons in DM halos[69]. The flattening occurs so that the initial angular momentum of the collapsing cloud is conserved. As the disk grows, inner regions form first, followed by the outer parts. This is referred to as the inside-out scenario of disk assembly. However, the hierarchical scenario of galaxy mergers does not completely explain the assembly of present-day disk galaxies. This is because it predicts larger sizes and numbers of spheroids than observed[70]. Instead, the assembly of disk galaxies at high redshift is believed to proceed via a clumpy phase in turbulent

gas-rich disks which is accompanied by smooth gas accretion[24, 71, 72]. In fact, previous studies suggest that cold gas accretion could have been the leading pathway of galaxy mass assembly[73, 74]. However, mergers also play an important role in providing a fresh supply of cold gas for subsequent star formation. There is observational evidence at intermediate redshifts indicating that when two gas-rich disk galaxies of similar masses merge (major merger), the resulting remnant may also be a disk galaxy[75–77]. Numerical simulations support this idea, predicting that disk galaxies can form in major wet mergers (when large amount of gas is involved) [78–81]. Additionally, minor mergers, where one galaxy is smaller than the other, have been shown to be more important than major mergers, and the rate of minor mergers increases as redshift decreases[82]. In addition to the formation and growth of the global disk, as mentioned above, features such as bars, bulges and spiral arms arise, grow and sustain out of local disk instabilities over time.

1.4 Galaxy evolution: A general perspective

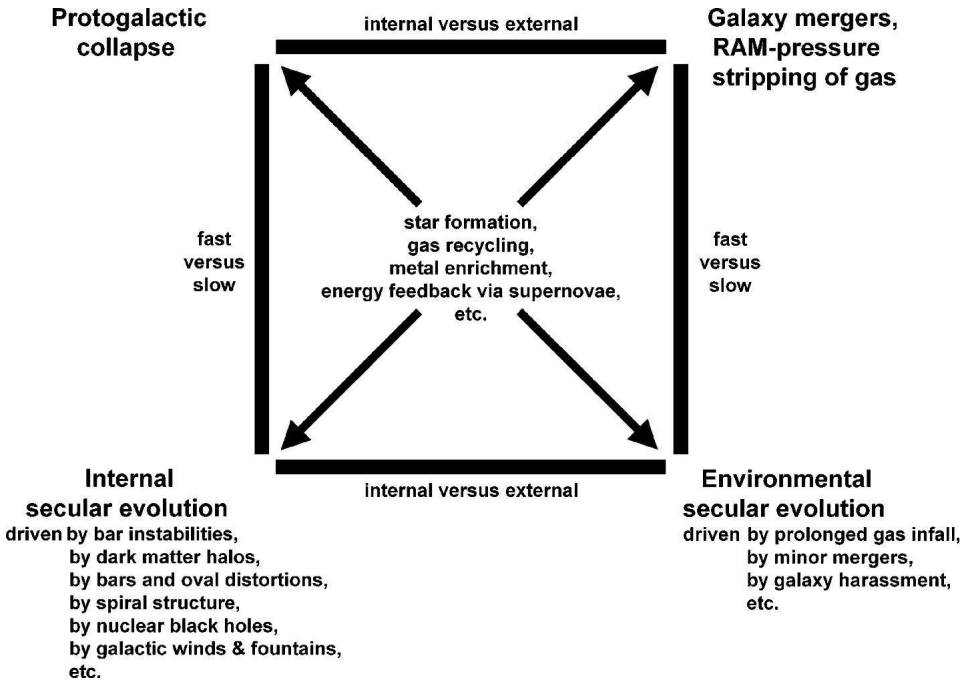

Figure 1.6: **Different processes involved in the assembly and evolution of galaxies.** Schematic depicting various processes involved in the assembly and evolution of galaxies. Processes on the left are those that happens within a galaxy and those on the right are those that are of external origin. Credit: Kormendy and Kennicutt (2004)[83].

One of the primary objectives in the study of galaxies is to understand how the processes governing the formation and evolution of galaxies across cosmic time led to the diversity of galaxies in the present day. But given the range of evolutionary timescales over which galaxies evolve, it is a challenging task to track them over Hubble time. A number of processes and factors influence the growth and evolution of a galaxy over its lifetime which is depicted well in a concise form in Figure 1.6 [83]. As depicted, the processes influencing a galaxy's evolution can be internal as well as external and fast or slow. A process can be considered fast when the timescale is comparable to its dynamical or free-fall time given by $t_{dyn} \sim (G\rho)^{-1/2}$, where G is the gravitational constant and ρ is the density of the mass distribution. Whereas it is a slow process if it is several times larger than this.

1.5 Dwarf galaxies: Small yet important

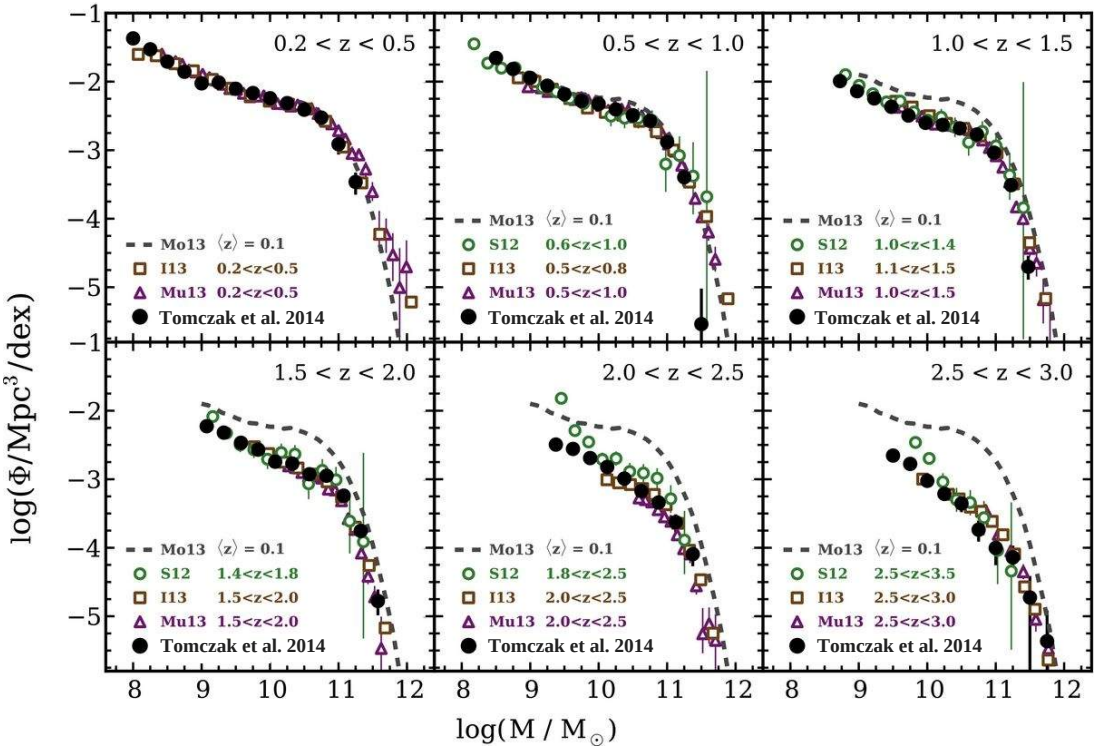

Figure 1.7: **Stellar mass functions at intermediate and high redshifts.** It shows the galaxy stellar mass functions (number density of galaxies vs stellar mass) in the redshift range 0.2 - 3.0. Additionally, it shows the quick buildup of low mass galaxies in the present epoch known as *'downsizing'* which we discuss in 1.6. We refer the reader to Tomczak et al. 2014[84] for further details. Credit: Tomczak et al. 2014[84].

The hierarchical assembly scenario of structures in our Universe suggests that smaller galaxies have merged to form the massive ones[9]. So low-mass galaxies, or commonly dwarf galaxies, play a pivotal role in the study of the assembly and evolution of galaxies. Dwarf galaxies are very common objects in the Universe[85], as indicated in Figure 1.7, over a wide range of redshifts. These are usually dark mater dominated systems[86] but they do not always follow model predictions. Unlike the cuspy DM profiles predicted by models[87, 88] they are likely to be cored[89]. Some dwarf galaxies like BCDs can have cuspy profiles as well[90]. Various criteria based on luminosity have previously been employed to define dwarf galaxies. Among these definitions, they are usually defined as those fainter than $M_B \sim -18$ mag [91] or $M_i - 5\log h_{100} > -18$ mag. Another criteria used to identify dwarfs is to have $M_g > -19.12 + 1.72(M_g - M_r)$ mag[92]. From a dynamical perspective, they are also defined as galaxies that have an asymptotic velocity in the flat part of the rotation curve ≤ 100 km s^{-1} [93]. In terms of stellar content they are typically considered to have masses less than 10^9 $M_\odot$[94].

An accurate picture of dwarf galaxy formation and evolution is still incomplete. On one hand, observations of dwarf galaxies have challenged the predictions of existing galaxy formation models with the 'missing satellite', 'too-big-to-fail' and 'cusp/core' problems [95]. On the other hand, the discovery and properties of ultra-faint dwarfs[96–98] and ultra diffused galaxies[99–101] raise questions on their structural assembly and the role of DM in their star formation and mass assembly histories. All the above may warrant a need to reformulate the physical models in order to better explain the observations. Additionally, star-forming dwarf galaxies are believed to be primary drivers of reionization in the Early Universe[102–107]. In fact, their low redshift analogs such as Green Peas (GPs)[108] and Blueberries (BBs)[109] have been extensively seen to emit ionizing Lyman continuum (LyC) and Lyman α (Lyα) photons[110–112]. A multitude of work has been done to understand the assembly history and evolution of the Local group of dwarf galaxies [113–115] but the intermediate and high redshift regime remains open for exploration.

1.6 Current understanding of dwarf galaxies

Advancements in telescope capabilities have allowed the detection and study of the faint and small galaxies manifold; revealing uncharted territories that provide unique opportunities to understand the processes driving galaxy formation and evolution. One of the immediate pressing questions to be answered in dwarf galaxy research is how are the diverse class of dwarf galaxies connected to each other. Many studies have tried to address this question in the past. For example, dIrrs have been proposed[116] to undergo a number of starburst phases, each lasting around 10^7 years[117], leading to their identification as BCDs and then fading away into faint dEs due to gas depletion or gas removal due to external factors[116, 118]. This however is still not quite clear as different studies have conflicting results[119–122].

The tension in their evolutionary scenario is not only seen among different classes but also among those belonging to the same class of objects. For example, dwarf spheroidals of the Milky Way differ from those of the M31 [123]. Contrary to previous studies [124–128], dwarfs in the Virgo cluster have revealed a bimodality in their kinematics which show rotationally supported dSphs [129–131] predominantly in the outer reaches of the cluster [132, 133]. Additionally, some early-type dwarfs are also similar in colour, age and metallicity with late-type galaxies [130, 134]. Such observations are indicative of ram pressure stripping wherein gas-rich, star-forming dwarfs can transform into early-type dwarf galaxies [133, 135, 136]. However, there are also isolated early type dwarfs [99, 100, 137] which are more likely to be self-regulated via stellar feedback mechanisms [138] or end products of possible brief interactions in the past[101]. In contrast to the early-type dwarfs, late-type or star-forming dwarf galaxies (SFDGs) are quite common [139, 140], gas-rich and usually metal-poor[4] systems. These are mostly seen in less crowded environments [141, 142] and the driving forces of evolution would most likely come from stellar activity. Dwarf galaxies are seen to have a wide range of star-formation rates reaching high values ($\sim$30 - 60 $M_\odot yr^{-1}$)[108, 143] and in extreme cases upto 123 $M_\odot yr^{-1}$[144] and specific SFR values of $\sim 10^{-9}$ - 10^{-7} yr^{-1}[143]. Such intense star formation within short timescales, termed as star-

burst, and production of short-lived massive stars lead to frequent supernovae (SNe) which greatly influences the interstellar medium (ISM) and sometimes even the intergalactic medium (IGM) [145–149]. For example, the effects of intense stellar activity can manifest as galactic winds[150], expanding X-ray plumes[151, 152] or even quenching of star formation[153–155]. Starburst triggers in dwarf galaxies have been explained due to gas infall[156, 157], infalling gas clouds[158], mergers[159] or in some cases intense stellar feedback[160–163]. On the other hand, some local SFDGs have shown that despite being gas-rich systems, they form stars very slowly[28, 164]; possibly in a self-regulated manner[165] and that feedback has less effect on their star formation at present times[166–168]. Therefore stellar feedback mechanism and its contribution still calls for a better understanding[169–171] which will subsequently provide insight into various physical processes such as photoionization, SFR density, winds, escape of ionizing photons, etc. [172–181].

Another interesting and important observation revealed by the star-formation histories of galaxies is the *downsizing* effect - wherein bulk of the star formation at earlier epochs was concentrated in massive galaxies which at present times has shifted to dwarf galaxies[182–188]. This at first glance appears to be at odds with the hierarchical models of galaxy formation because the downsizing effect would imply that massive galaxies assembled at earlier times. Models suggest that somehow the star formation in the low mass galaxies should be suppressed or delayed at earlier epochs[189]. Possible factors include contribution from background UV radiation[190, 191] or periodic gas outflow/inflow over cosmic time due to supernova explosions (e.g. [138]). Nevertheless, the picture of downsizing in the light of the ΛCDM framework remains to be understood.

The overall metallicity and spatial variation can provide important clues to the evolutionary state and the history of galaxies. Some early-type dwarfs are seen to exhibit strong spatial metallicity gradients[192, 193]. However, SFDGs show a flattening of their metallicity profile[114, 194]. This is believed to be the result of blowing out of enriched gas from the central star-forming regions of disk galaxies which *rains* back onto itself like a *fountain*, thereby homogenizing the metallicity[146, 148, 195–198]. Another study explains this

due to something called as a *centrifugal barrier mechanism* where the rotation of the galaxy exerts a centrifugal force on the inward moving gas. As a result, star formation occurs homogeneously throughout the galaxy and constantly over cosmic time to produce the flat metallicity profiles[199].

The mass/luminosity-metallicity relation is one of the fundamental empirical relations observed in galaxies since long[200–205] and provides insight into the history of their evolutionary drivers. The Local Group dwarf galaxies have shown that metallicity decreases with decreasing stellar mass, albeit there is a flattening above $\sim 10^{10.5}$ $M_{\odot}$ [203, 206–208], with an increased scatter at increasingly fainter magnitudes[98]. Such an observation has been interpreted to be the result of stellar feedback that effectively blows out metals from shallow potential wells of low mass galaxies[138, 203, 209–215]. Other processes such as gas accretion from the surrounding intergalactic medium (IGM), tidal stripping may also alter the metallicity or produce scatter in the mass/luminosity-metallicity relation in these systems [98, 216–219]. However, a detailed understanding of the MZR in the low-mass regime was constrained mostly to the nearby Universe. Studies of high redshift galaxies in the Early Universe were mostly possible for massive galaxies[220–240]. These studies show that massive galaxies follow a decreasing trend in metallicity with redshift at fixed stellar mass. Very recently, *JWST* NIRSpec observations of low-mass galaxies (as low as $\sim 10^{6}$ $M_{\odot}$) show a flattening of the MZR with redshift at fixed stellar mass[241, 242]. Surprisingly, the MZR becomes shallower below $\sim 10^{9}$ $M_{\odot}$ which is not indicated by other studies (e.g. [203, 229]). This essentially implies that there are several different factors which drive the observed relation in different ways, including a dependency on the galaxy mass[170, 214, 243–246]. To understand the contribution of each factor, it is required to study representative samples of galaxies based on their environment, morphology or other physical/chemical properties.

So far we have seen that the richness of physical and chemical properties in dwarf galaxies make them great laboratories to better understand the contribution of different processes and environmental conditions towards the assembly and evolution of galaxies. It is important to note that detailed dwarf galaxy research has been dominated by the study of those residing in the low redshift

Universe. Much of the understanding of the high redshift dwarfs has been drawn from simulations based on observations and understanding of nearby dwarfs or faraway massive galaxies.

1.6.1 Blue Compact Dwarf galaxies

Figure 1.8: **I Zwicky 18.** Image of a nearby prototype BCD (center). There is however another galaxy (top) associated with I Zwicky 18 implying interaction[247]. This thesis primarily talks about isolated BCDs. Credits: NASA, ESA, Y. Izotov (Main Astronomical Observatory, Kyiv, UA) and T. Thuan (Univ of Virginia)

We now bring our attention to BCDs, which we primarily target in this thesis. As we mentioned above, these are often considered as a phase in dwarf galaxy evolution (e.g. [116, 118, 121, 248]. They are low-luminosity, $M_K > -21$ mag[3], metal-deficient ($\frac{1}{50}$ $Z_\odot \leq Z \leq \frac{1}{2}$ $Z_\odot$)[4] and star-forming (10^{-3} - 10^2 $M_\odot$ yr^{-1})[249] dwarfs with an intense centrally concentrated burst of

recent star formation[250]. Some BCDs are also seen to exhibit extremely low metallicities $7.0 \lesssim 12+\log(O/H) \lesssim 7.6$ and are termed as extremely metal-poor BCDs (XBCDs). They usually have turbulent gas disks[251–254] and are clumpy like high redshift galaxies[23, 71, 255–258]. All such properties mentioned above make them good analogues to primordial galaxies. With little dust[259], blue optical colours emitted by massive O and OB spectral type of stars[20, 260–262] are easily observed and the galaxy spectrum is characterised by narrow and strong emission lines[263]. Apart from these types of stars, they also contain highly evolved and short-lived Wolf-Rayet stars[264] characterised by strong winds blowing away their surface material.

BCDs were initially believed to be young galaxies due to their blue optical colours and evident recent star formation. However, it was later discovered that underneath the central star-forming region, lies an extended disk containing an older population of low-mass stars[120, 261, 265]. The old disk constitutes a low surface brightness (LSB) component due to low stellar surface densities, and typically extends beyond a surface brightness of $\mu_B \geq 24$ mag arcsec^{-2}[261, 266]. This underlying LSB disk is often referred to as the 'host' and is believed to play a crucial role in regulating the star formation in these galaxies[26, 120, 248, 267, 268]. Studies in the past have compared the LSB host with 'true' LSB galaxies. It is seen that the BCD hosts are unique, when compared to LSB galaxies, and are brighter and more compact than the latter[122]. But a potential connection between BCD hosts and LSB galaxies cannot be ruled out[248].

The intense star formation in BCDs implies the conversion of large amounts of gas, present in these systems, into stars[251, 263, 269]. Extensive research has revealed that BCDs typically host extended HI disks[251, 270–275] which can extend up to 3-4 times the size of their optical disks. Additionally, studies have identified filamentary structures[157, 251, 276–279] or large HI halos[280], and higher HI densities concentrated near the central starburst regions of these galaxies. Despite the wealth of observational evidence regarding the gas content and distribution within BCDs, the triggering mechanism responsible for star-formation in BCDs remains elusive[5, 26, 273, 281]. Studies have proposed various scenarios to explain the onset of these star-formation events, such as

interactions and mergers[159, 282–285], tidal disruption[159, 273, 286–289], gas accretion[12, 22, 290] or in-falling gas clumps[26, 291].

Although BCDs are considered to be an evolutionary phase among different dwarf classes, various studies in the past have drawn different conclusions. On one side BCDs, dEs with star formation and dIrrs are considered to be distinct systems[119] and another scenario believe that dIrrs turn into BCDs as a result of high star formation that would convert into dEs upon exhaustion of fuel[116]. Similarly, there are other studies that are in conflict with one another[120–122, 248, 252, 292], thereby indicating the need for further investigation. The episodic nature of star formation, separated by extremely long intervals of time (∼1 Gyr or so)[293], also raises a number of questions about their stellar mass growth, star-formation history, and the overall evolution.

Simulations investigating the formation of BCDs suggest that they form via the merging of gas-rich dwarf galaxies[282, 284] and are surrounded with extended gas disks. Additionally, simulations predict the transformation of ultra-compact BCDs, formed during mergers, into nucleated dwarfs as the young stars gradually fade over time[294]. Using these merger scenarios, studies also try to explain the observed steep central rotation curves in these systems, which is likely due to the high gas concentration in the inner regions. Notably, the formation of BCDs could be intricately linked to the strength of the interactions involved; a mere tidal interaction without merger is insufficient to form BCDs[284].

While most of the existing studies on BCDs predominantly focus on interactions with companion galaxies or crowded environments, the investigation of isolated BCDs, i.e. those outside such environments and also referred to as ‘field’ BCDs, may offer valuable insights into whether these formation mechanisms hold universally true for all BCDs. In these isolated or cluster-free environments, factors such as gas accretion from cosmic filaments[295] and disk instabilities[25, 26, 291] may play significant roles, whose contribution otherwise is not quite clear. Whether the assembly and evolution of BCDs also follow the same route[60, 296] as that of massive galaxies is an open question.

1.7 Multi-wavelength Observatories

For the work presented in this thesis, we have made use of ultraviolet (UV), optical and near-infrared (NIR) imaging observations from ground-based as well as space-based telescopes. In the following we present a brief overview of these observatories.

1.7.1 AstroSat

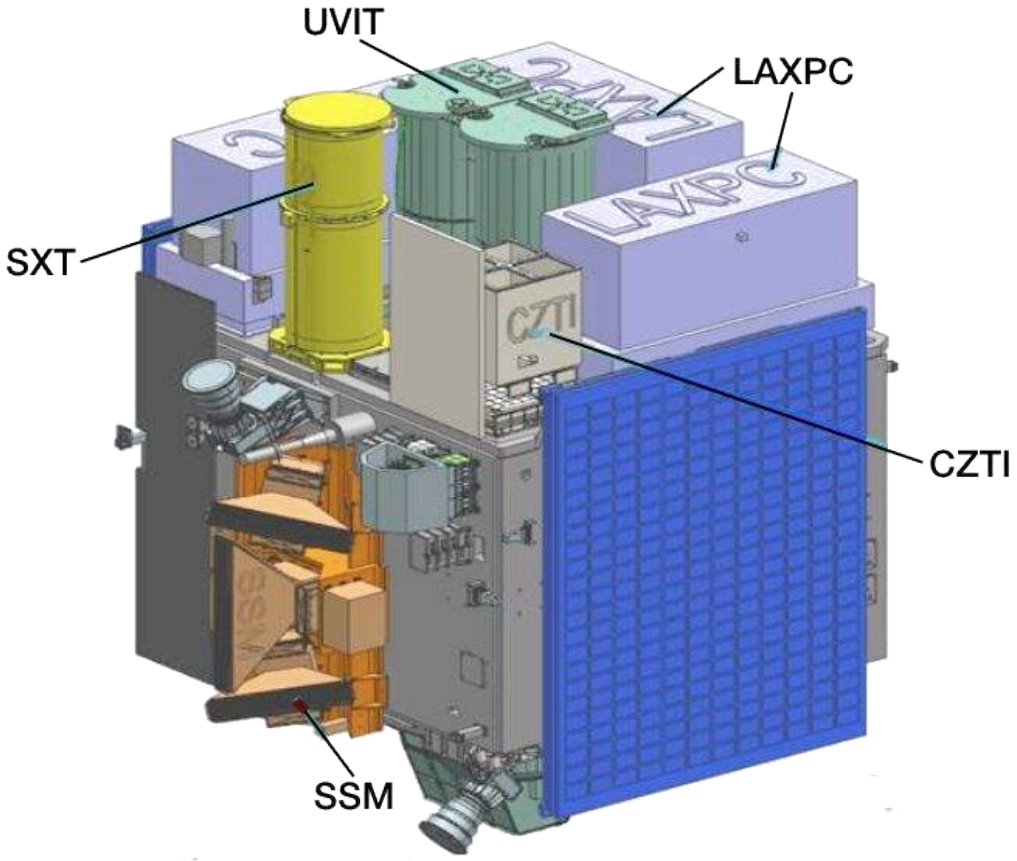

Figure 1.9: **AstroSat.** Schematic showing the different payloads onboard AstroSat, Credit: http://astrosat.iucaa.in/

India's first multi-wavelength space based observatory, the *AstroSat*[7], was launched by the Indian Space Research Organisation (ISRO) on September 28, 2015. The primary objectives of the observatory included the study of highly energetic binary systems and extragalactic phenomena, active galactic nuclei (AGN), transient X-ray sources and medium-resolution large-scale UV surveys. The observatory consists of five payloads, viz. the Large Area X-ray Proportional Counters (LAXPC, 3 - 80 keV), Cadmium-Zinc-Telluride Imager

(CZTI, 10 - 100 keV), Soft X-ray imaging Telescope (SXT, 0.3 - 8 keV), Scanning Sky Monitor (SSM, 2.5 - 10 keV) and Ultra-Violet Imaging Telescope (*UVIT*, 1300Å - 5500Å).

The *UVIT*[6] houses two co-aligned Ritchey–Chretien telescopes having an aperture size of ∼375 mm that images in the FUV (1300 - 1800Å), NUV (2000 - 3000 Å) and visible (VIS, 3200 - 5500 Å) channels. The VIS channel is primarily used for drift tracking due to low UV photon count rates. A filter wheel for each channel selects from the appropriate broadband filters for observations [297]. With a full field of view (FoV) of 28′ diameter, intensified complementary metal-oxide semiconductors (CMOS) detectors having a dimension of 512x512 pixels are used. These are mapped onto a subpixel grid of 8x8 resulting in a plate scale of ∼0.416″ per subpixel. The spatial resolution is 1.3″-1.5″ in FUV, 1.2″-1.4″ in NUV and 2.5″ in VIS channels[297]. Apart from imaging, the *UVIT*[6] is also equipped with gratings (one for NUV and two for FUV) for performing low-resolution slitless spectroscopy. The schematic of AstroSat[7] with its payloads is shown in Figure 1.9. In this work we have made use of deep *UVIT* imaging observations (P.I. Kanak Saha, ID: GT05-240).

1.7.2 Hubble Space Telescope (HST)

The *HST* (Figure 1.10), named in honour of astronomer and pioneer of extragalactic astronomy, Edwin Hubble, is one of NASA's Great Observatories and launched into space in April 24, 1990 onboard the Space Shuttle *Discovery*. It is a Ritchey–Chretien Cassegrain telescope with a primary mirror size of 2.4 m diameter and observes in the UV, visible and NIR wavelengths. Currently, the *HST* has four instruments in operation, viz. Advanced Camera for Surveys (ACS), Cosmic Origins Spectrograph (COS), Space Telescope Imaging Spectrograph (STIS) and Wide Field Camera 3 (WFC3). The ACS two channels - (a) Wide Field Channel (WFC) with the largest FoV of 202″ x 202″ is capable of optical imaging, slitless spectroscopy and spectro-polarimetry in the wavelength range 3500 – 11000 Å. (b) The Solar Blind Channel (SBC) can perform FUV imaging and slitless spectroscopy in the wavelength range 1150 – 1700 Å. The COS can perform both medium and low-resolution spectroscopy using multiple gratings onboard in FUV (900 - 2050 Å) and NUV (1650 - 3200 Å)

Figure 1.10: **Hubble Space Telescope** prior to its deployment after the first servicing mission. Credit: nasa.gov.in

wavelengths. The STIS can perform both imaging and spectroscopy using its Multi Anode Microchannel Array (MAMA, in FUV and NUV) and CCD coupled with gratings and prisms. It broadly operates in the range 1150 - 11000 Å. The WFC3 also offers imaging and spectroscopic capabilities in the wavelength range 2000 - 17000 Å. The spatial resolution in imaging ranges from ∼0.1" - 0.2"[298, 299] and has a pixel scale of 0.03 mas or 0.06 mas [300] in the reduced images. With the extended period of time in operation, the *HST* has delivered some spectacular results and understanding of the Universe such as the discovery of the farthest star ever seen[301], one of the farthest confirmed galaxies using its deep field surveys (GN-z11) [40] (the farthest confirmed is by the new James Webb Space Telescope, GS-z-13-0 [302]), the constraining of the age of the Universe, the study of proto-planetary disks, to name a few. Here we have made use of *HST*'s archival, deep optical and NIR imaging observations[303].

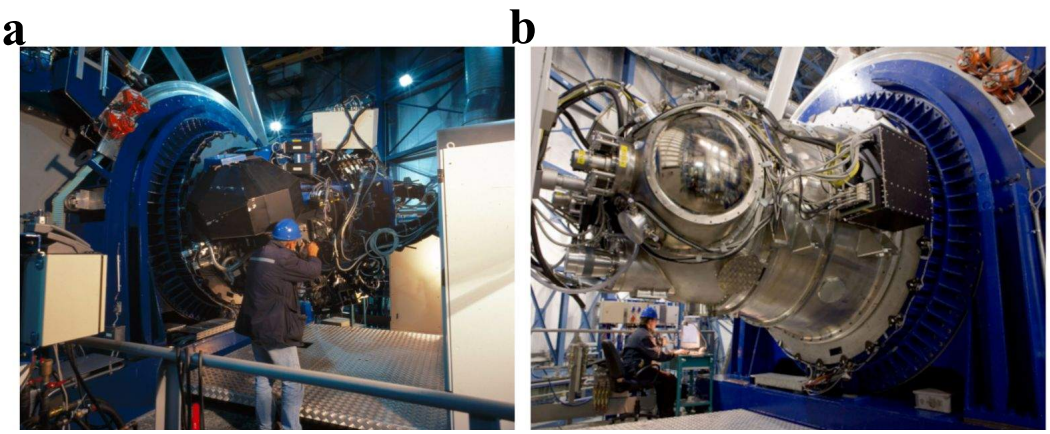

Figure 1.11: **The Very Large Telescope. a**: Showing a picture of *VIMOS* under inspection. Credit: ESO. **b**: Showing a picture of the *HAWK-I* onboard the VLT. Credit: ESO/H.H.Heyer

1.7.3 Visible Multi-Object Spectrograph (VIMOS)

The *VIMOS* (Figure 1.11, left) is a ground-based instrument mounted on the Nasmyth focus B at Very Large Telescope Unit Telescope 3 (VLT-UT3) with its 8.2 m diameter mirror at Paranal. It operates in the wavelength range 3600 - 10000 Å and functions as a wide-field imager as well as a multi-object spectrograph. The instrument is again made up of four arms each having a FoV of $7'$ x $8'$ and pixel scale of $0.205''$. Multi-object Spectrograph using slit masks allows for a moderate resolution spectroscopy (R$\sim$200-2500). Additionally, it also contains an Integral Field Unit (IFU) with similar resolving power to the MOS. In our work, we make use of publicly available deep R band imaging data.

1.7.4 High Acuity Wide-field K-band Imager (HAWK-I)

HAWK-I (Figure 1.11, right) is a ground-based NIR imaging instrument[304] developed at ESO and installed on one of the Nasmyth foci at the VLT-UT4. The detector is composed of four 2k x 2k Rockwell HgCdTe Molecular Beam Epitaxy (MBE) HAWAII 2 RG arrays and has a FoV of 7.5 x 7.5 $'$ and pixel scale of 0.1 $''$. The camera operates in the wavelength range 0.9 - 2.5 μm with its set of broadband and narrowband filters[304]. The image quality is decent with a seeing value of $\sim$ 0.38 - 0.5 $''$ [305]. We have utilized its publicly available deep imaging in the K_s band ($\sim$2.15 μm).

1.7.5 The DESI Legacy Imaging Survey

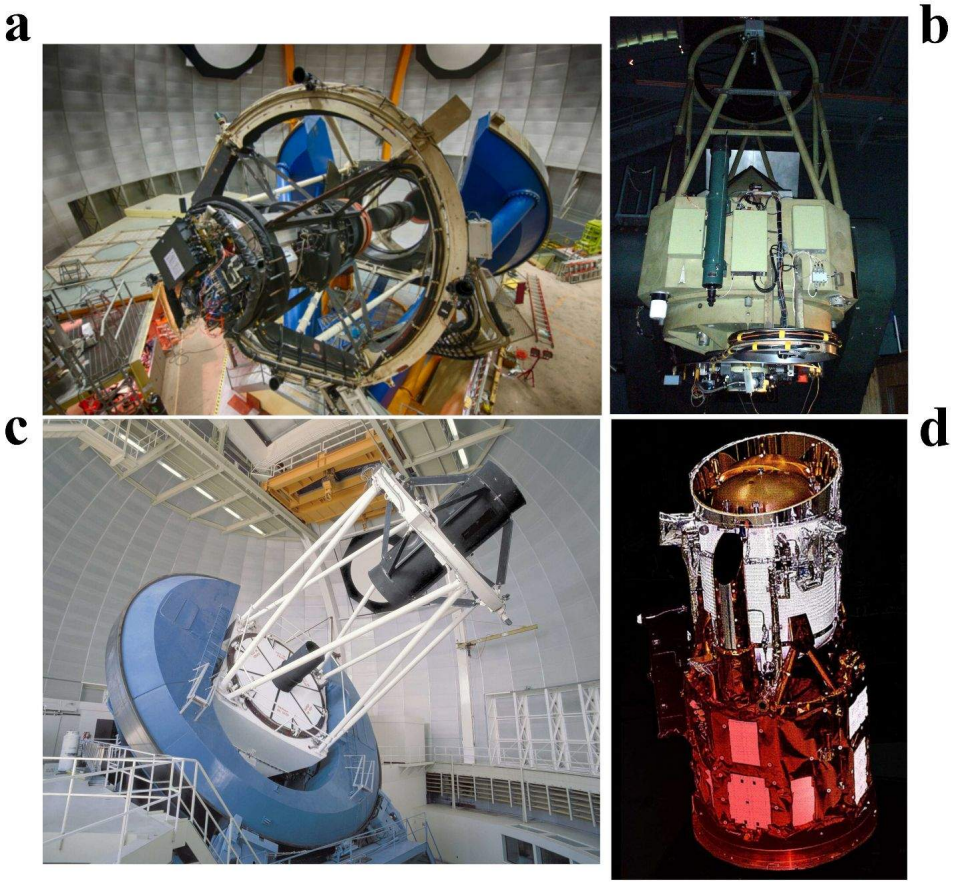

Figure 1.12: **The DESI Legacy survey telescopes.** *DECam* (**a**, on the Blanco 4m telescope at CTIO, source: www.darkenergysurvey.org/the-des-project/instrument/the-camera/), Bok Telescope (**b**, source: wikimedia commons), the Mayall telescope (**c**, Credit: NOIR-Lab/NSF/AURA), the WISE telescope (**d**, Credit: jpl.nasa.gov)

The Dark Energy Spectroscopic Instrument (DESI) Legacy survey[306] performed dedicated imaging of the sky (>14000 sq degrees) in the g, r and z optical bands. It utilises three different telescopes, viz. the Dark Energy Camera (*DECam*) on the 4 m Blanco telescope at the Cerro Tololo Inter-American Observatory; the University of Arizona Steward Observatory 2.3 m (90 inch) Bart Bok Telescope at Kitt Peak National Observatory; and the Mayall 4 m Telescope at the Kitt Peak National Observatory. Now, it has also incorporated additional public *DECam* data which expanded its observation to >20000 sq degrees. The three surveys image the sky in g,r,z; g,r; and z band respectively covering ∼400-1000 nm wavelength range. The survey also combines data from the four infrared bands of the Wide-field Infrared Survey Explorer satellite at 3.4 μm, 4.6 μm, 12 μm and 22 μm. We have utilised the publicly available g,

r and z band imaging from the survey.

The transmission curves of all the broadband imaging observations used in this thesis is presented in Figure 1.13.

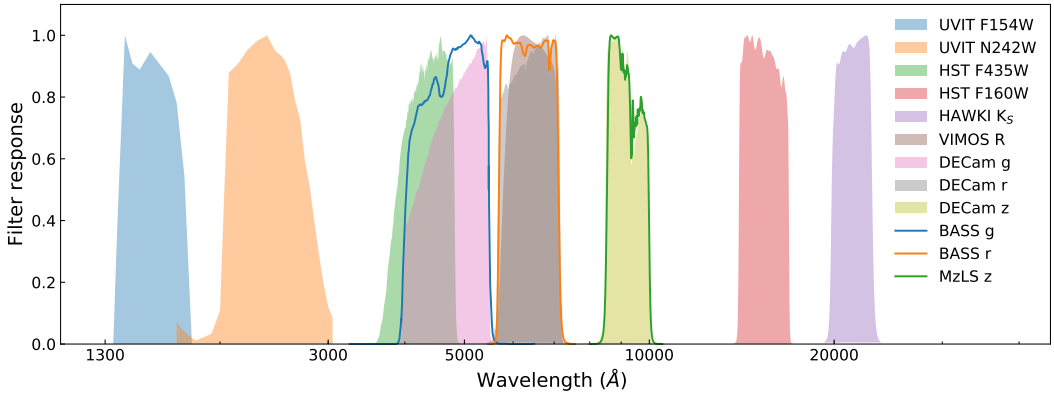

Figure 1.13: **Filter response curves of the observations utilized in this thesis.** The legends are sorted according to the wavelength regimes they cover. The legends BASS (g,r) and MzLS z refer to Beijing-Arizona Sky Survey with the Bok Telescope and Mayall z-band Legacy Survey with the Mayall telescope respectively.

1.8 Methods

I will briefly discuss the methodology and the tools used during this research as follows:

1.8.1 Surface Photometry

Photometry refers to the measurement of incoming photons from an astronomical source. Modern-day detectors convert the detections at different wavelengths into electrical signals which when calibrated with standard sources give us the apparent brightness of the objects under study. For point-like sources, we are mostly interested in the total magnitude of the objects. However, for extended objects like galaxies, the variation of light over the objects is important which can be used to infer their physical as well as chemical properties. This quantity is expressed as the brightness per unit area in the object and has units of magnitude per sq arcsec.

The analysis involves fitting ellipses to isophotes - which connect pixels of similar intensities, via an iterative procedure using the ELLIPSE task [307] in

the Image Reduction and Analysis Facility (IRAF) tool[308]. We try to give here a simple working mechanism of the algorithm. At first, we feed in the initial guesses for the geometric parameters of an ellipse - centre coordinates, ellipticity and position angle for an object in an image. The image is then sampled along an elliptical path with the initial geometric parameters and after least squares minimization of the quantity S below, the harmonic amplitudes (A_n, B_n) are obtained.

$$S = \sum_i [y_{ob}(\phi) - y(\phi)]^2 \tag{1.1}$$

where,

$$y(\phi) = y_0 + \sum_{n=1,2} (A_n \times sin(\phi)) + (B_n \times cos(\phi)) \tag{1.2}$$

Here ϕ is the azimuthal angle and y_0 is the average intensity of the elliptical path defined by the initial guess parameters. The harmonic amplitudes mentioned above are basically 'corrections' that control the shape and location of the fitted ellipse. At each semi-major axis (SMA) length, the minimization continues iteratively and stops once it reaches a minimum rms and gives a best-fit ellipse. After this, at the same SMA length, higher order harmonics can be fit ($n \geq 3$) that results in complex shaped ellipses as shown below in Figure 1.14 [309]. This procedure is carried out at different SMA lengths according to the step size specified by the user and for each subsequent SMA length, the initial parameters are the best-fit parameters at the nearest SMA. The output is a table containing the intensity and other best-fit parameters as a function of SMA length. We have used v2.16 of the tool in this thesis.

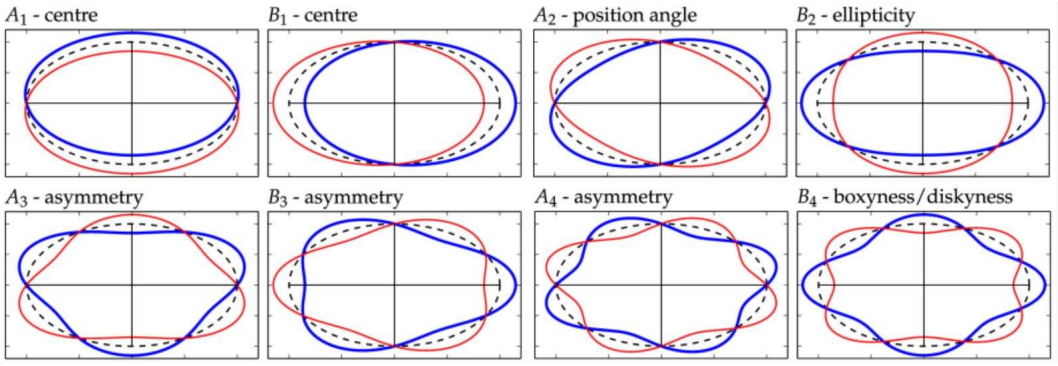

Figure 1.14: **Showing the significance of the first four harmonic coefficients (A_1, A_2, B_1, B_2) to an elliptical isophote**. Blue thick ellipse indicates a positive coefficient while red thin indicates a negative coefficient. The black dotted ellipse indicates the reference. Credit: Ciambur 2015[309]

1.8.2 PROFILER

This is a PYTHON-based GUI tool designed to analyse the 1D surface brightness profiles of galaxies [310]. It consists of a range of analytical functions used to model different components of galaxies such as the disk, bulge, bars, spiral arms etc. It can also take into account the point spread function (PSF), which produces a resultant blurring effect due to the optics of the telescope or atmospheric conditions (in the case of ground-based telescope), of the imaging data to obtain intrinsic galaxy structural parameters. We can directly use the output tables from the IRAF ELLIPSE task and feed into PROFILER without any processing which makes it very user-friendly. Once we have decided the components that we want to fit, it performs a least square minimisation of the quantity $\sqrt{\sum_i(\mu_{obs} - \mu_{model})}$ using the PYTHON LMFIT[311] package incorporating the Levenberg-Marquardt algorithm [312]. For a detailed description of the tool, we refer the reader to Ciambur 2016[310]. We have used v2.0 of the tool in this thesis work.

1.8.3 Source Extractor

Source Extractor (*SExtractor*) [21] is an automated standalone tool to analyse large-scale imaging observations within a short span of time. In that, it can perform tasks ranging from background estimation, source detection, decent deblending in moderately crowded fields, and photometry to extended/point source classification. As output, it can provide various check files such as background images, rms images, and detection images to name a few. The basic process of using the tool starts off with specifying a configuration file for *SExtractor*. Then the tool starts scanning the input image and creating a mesh grid over it to estimate the sky background. After background subtraction, it starts detecting sources based on the criteria specified in the configuration file, viz. minimum intensity value required by any pixel to be considered that it belongs to a source and the minimum number of connected pixels above the threshold. It can also use filters for smoothing as per requirements to perform detection. For separating blended objects in the image, based on our defined deblending parameters, *SExtractor* constructs a tree of objects

by creating different brightness levels within an object. Now, if there are at least two branches in the tree whose integrated flux is above a certain fraction of the flux of the whole object, two different objects are said to have been detected. Additionally, it can also clean out faint artifacts in the vicinity of bright objects by subtracting the contribution from the wing of the bright source and reconsidering the faint detection. Finally, it does photometry in several ways and measures the shapes and sizes of the objects and produces an output catalog containing all parameters as requested by the user.

1.8.4 Noise Chisel

Noise Chisel [313, 314] is a part of GNU Astronomy Utilities or Gnuastro, which is another automated tool with capabilities similar to SExtractor as described above. SExtractor is a signal-based detection tool but Noise Chisel's detection algorithm is based on the noise estimate of the background. This has been designed to find faint signal over a noisy background and at the same time avoid false detections which is otherwise an issue with SExtractor. The threshold is designed to be independent of the background and estimated from the cumulative pixel distribution of the image. It converts the input image into a binary-valued image - identifying a pixel as either background or source pixel. The tool then separates the source pixels into separate objects based on their connectivity. It then helps remove false detections by re-analyzing the pixels belonging to the background and foreground (source pixels). We refer the reader to the source material[313, 314] for an in-depth description.

1.8.5 FAST

Fitting and Assessment of Synthetic Templates or FAST is a Spectral Energy Distribution (SED) fitting code developed by Kriek et al. (2009)[315] to obtain the physical properties of the targets of interest. It can make use of broad-band photometry, spectra, or both. Through a parameter file, the choice of stellar population synthesis (SPS) model, the initial mass function(IMF), dust extinction law and a grid of stellar population properties - stellar population age, star-formation timescale, extinction, metallicity, and redshift, are fed into the code. The range and step sizes for these properties need to be specified to

generate a grid of model SEDs. The best-fit model chosen is the one with the lowest χ^2 value.

1.8.6 STARBURST99

This code is used to predict observable properties of star-forming galaxies and was developed by Leitherer et al. (1999)[32]. It makes use of either a continuous star formation with a specified SFR or an instantaneous star formation to generate a specified stellar mass and a single stellar population (SSP). The stellar population is then evolved over a specified time as per the stellar evolutionary models and other factors that include metallicity, IMF, stellar mass, stellar wind model and more. After the simulation, we can obtain a number of physical parameters at each time step such as the number of ionizing photons, the amount of elements ejected during stellar winds and supernovae, emission line strengths, the spectrum, colours and magnitudes, etc. An in-depth detail on the working and usage of the code can be obtained from the parent paper[32]. Here we use v7.0.1 of the code which is publicly available as a web-based tool at https://www.stsci.edu/science/starburst99/.

1.8.7 GALFIT

GALFIT[316, 317] is a tool that fits 2D analytical functions to galaxy images directly to obtain their structural parameters. It assumes that all sources can be represented by generalized ellipses given by:

$$r(x,y) = \left(|x-x_0|^{C_0+2} + |(y-y_0)/q|^{C_0+2}\right)^{1/(C_0+2)} \tag{1.3}$$

where (x_0,y_0) is the centroid of the ellipse, C_0 is a constant that controls the shape of the ellipse. $C_0 = 0$ produces pure elliptical isophotes. For decreasing C_0 ($C_0 < 0$), isophotes become more disky while for an increasing C_0 ($C_0 > 0$) they become more boxy. q is the axis ratio of the elliptical isophote. The ellipse can also be oriented to any position angle (θ_{PA}). For flexibility and better decomposition of structures, regular elliptical isophotes can be modified by adding perturbations to the generalized ellipse such as Fourier modes, bending modes or truncation. During the process, the algorithm first cuts out a section

of the input image as specified by the user. The models to be used for fitting are first convolved with the supplied PSF image and a χ^2 minimization using the Levenberg-Marquardt[312] is performed to obtain the models along with the necessary fitted parameter files. It comes with a number of analytical functions such as the Sersic, exponential, de Vaucouleur, Nuker, Gaussian, etc. to model different components of a galaxy.

1.9 Outline of the thesis

Understanding the assembly and evolution of dwarf galaxies over cosmic time is of utmost importance to complete the picture of galaxy evolution. Also, targeting dwarf galaxies beyond the Local Universe (>100 Mpc) is of prime importance to sample young galaxies that are in an actively growing phase. Keeping this goal in mind, we study a sample of BCDs at redshifts $0.1 \leq z \leq 0.24$ ($\sim$ 380 - 780 Mpc) which correspond to lookback times of 1.3 - 2.8 billion years in standard cosmology. Our sample lies in the *GOODS-South* field for which we have recently obtained deep ultraviolet (UV) observations (Saha et al., *in preparation*) with the *Ultra-Violet Imaging Telescope (UVIT)*[6]. With these novel UV observations, combined with archival optical and NIR data, we study the assembly and growth scenario of BCDs. We also propose and obtain FUV observations for nearby BCDs to further understand their evolution over time.

In *Chapter 2* of the thesis, I present and discuss the analysis of the multi-wavelength morphologies of our BCDs based on *UVIT*[6] and *HST* imaging observations. These observations, for the first time, reveal the presence of extended ultraviolet (XUV) disks in these distant BCDs and imply an ongoing assembly of the outer stellar disk over the past 100 million years or more.

We observe massive FUV clumps of the order 10^6 $M_\odot$ (estimated from FUV fluxes; $\sim$ 1 % of total galaxy masses) in the outskirts of these BCDs. In *Chapter 3*, I discuss the detection and robustness of the clumps and the timescales for inward clump migration and clump driven disk evolution due to dynamical friction[26]. These massive clumps will migrate inwards over a Gyr or so. The whole outer disk would not come in within a Hubble time and

likely result in extended old stellar disks as seen in local BCDs[27].

In *Chapter 4*, I present the outer star-formation rate surface density (SFRD) measurements and broadband UV colours. We perform stellar population modelling using STARBURST99 code[32] and estimate stellar ages in the outer disk. We are able to measure SFRDs down to 10^{-5} - 10^{-6} $M_{\odot}yr^{-1}kpc^{-2}$ which would translate to gas densities of the order $\sim$1 $M_{\odot}pc^{-2}$ or less. Outer, low-density star-forming regions serve as excellent sites for understanding primordial star formation.

XUV disks in local BCDs have not been discussed extensively in the literature. Our results from intermediate redshift BCDs motivate us to probe if this is a mere case of non-detection or if present-day BCDs have evolved beyond their XUV phase. In *Chapter 5*, I describe the observations carried out for a sample of low redshift BCDs using *AstroSat/UVIT* (P.I. Anshuman Borgohain, ID: A10-123) and present our preliminary results.

I finally conclude the thesis with our key results and elucidate their implications and prospects for future work in *Chapter 6*.